Cement and Concrete Research 39 (2009) 171–181

Contents lists available at ScienceDirect

Cement and Concrete Research

journal homepage: http://ees.elsevier.com/CEMCON/default.asp

Integration approach of the Couette inverse problem of powder type self-compacting concrete in a wide-gap concentric cylinder rheometer
Part II. Influence of mineral additions and chemical admixtures on the shear thickening flow behaviour

G. Heirman [a,*], R. Hendrickx [a], L. Vandewalle [a], D. Van Gemert [a], D. Feys [b], G. De Schutter [b], B. Desmet [c], J. Vantomme [c]

[a] Reyntjens Laboratory, Department of Civil Engineering, K.U.Leuven, Kasteelpark Arenberg 40 b2448, B-3001 Heverlee, Belgium
[b] Magnel Laboratory for Concrete Research, Department of Structural Engineering, Ghent University, Technologiepark 904, B-9052 Zwijnaarde, Belgium
[c] Department of Civil and Materials Engineering, Royal Military Academy Brussels, Renaissancelaan 30, B-1000 Brussel, Belgium.

ARTICLE INFO

Article history:
Received 7 July 2008
Accepted 11 December 2008

Keywords:
Fresh concrete (A)
Rheology (A)
Admixture (D)
Filler (D)
Shear thickening

ABSTRACT

The influence of mineral additions and chemical admixtures on the shear thickening flow behaviour of powder type self-compacting concrete (SCC) is studied by means of a wide-gap concentric cylinder rheometer. The Couette inverse problem is treated by means of the integration method in order to derive the flow curve $\tau(\dot{\gamma})$ from the torque measurements.
According to the experimental results, the shear thickening effect is found to be strongly influenced by the addition of the chemical admixture (a polycarboxylate ether based superplasticizer), whereas mineral additions were found to modify the intensity of shear thickening. The limestone, quartzite and fly ash addition used in this research project, respectively increase, unalter and decrease the shear thickening intensity. The powder volume and the available amount of free water proved to have a major impact on the viscosity of the powder type SCC mixes. Increasing the powder volume or decreasing the amount of free water results in an increased viscosity of the SCC mix.

1. Introduction

In order to describe the shear thickening behaviour of powder type self-compacting concrete (SCC) in a wide-gap concentric cylinder, the theoretical background was presented in a first part of this publication [1]. The investigation in Part II is concerned with the influence of mineral additions and chemical admixtures on the shear thickening behaviour of powder type SCC, commonly used in Belgium. In case of (European) powder type SCC, the main properties of fresh SCC, i.e. a high flowability and a high resistance to segregation, are basically achieved by using, respectively, a chemical admixture and a mineral addition:

- The chemical admixture consists of a high range water reducing admixture, based on (modified) polycarboxylate ethers (i.e. a so-called 'third generation' superplasticizer) in order to achieve a sufficiently high flowability of the SCC mixture.
- The mineral addition is used in order to increase the total powder content without increasing the heat generation during cement hydration. In this way, the viscosity of the SCC mixture is increased compared to traditionally vibrated concrete (TC). European powder type SCC (having a total powder content of about 550–650 kg/m^3) mostly uses mineral additions like limestone powder, quartzite powder, fly ash or silica fume.

The flow behaviour of fresh SCC is mostly characterized by empirical test methods like slump-flow, V-funnel, L-box, sieve stability, etc. [2–4]. Because equipments for the above tests are inexpensive and tests are carried out easily, they are suitable for on site use. However, these tests do not provide a fundamental description of the concrete's flow behaviour. For the knowledge of the flow parameters, rheological measurements from a materials science approach by means of a rheometer are necessary.

2. Rheology and concrete technology

2.1. Rheological models in concrete technology

Fresh concrete is treated here as a fluid and, as a consequence, fluid rheology methods are used to describe the concrete flow. In this approach, only the motion of a 'large' number of solid particles is taken into consideration, without going into the detailed motion of every single one of them. In order to properly treat fresh concrete as a

* Corresponding author. Tel.: +32 16 32 16 79; fax: +32 16 32 19 76.
E-mail address: Gert.Heirman@bwk.kuleuven.be (G. Heirman).

0008-8846/$ – see front matter © 2008 Elsevier Ltd. All rights reserved.
doi:10.1016/j.cemconres.2008.12.006

fluid, a certain degree of flow (i.e. a slump of at least 100 mm, according to EN 12350-2:1999) must be achieved while the concrete stays homogeneous (i.e. no segregation may occur) [5].

The rheology of fresh concrete is usually described by the Bingham model, at least as a first approximation. In this model, the shear stress τ is assumed to be linearly proportional to the shear rate $\dot{\gamma}$, after exceeding a certain Bingham yield stress $\tau_{0,B}$:

$$\begin{cases} \tau = G^* \cdot \gamma (\text{or } \dot{\gamma} = 0) & \tau < \tau_{0,B} \\ \tau = \tau_{0,B} + \mu \cdot \dot{\gamma} & \tau \geq \tau_{0,B} \end{cases} \quad (1)$$

Below the Bingham yield stress, the fluid behaves Hookean, while it behaves Newtonian above. G^* and μ are called the '(complex) shear modulus' (Pa) and the 'plastic viscosity' (Pa·s) respectively.

The Bingham yield stress is *not* necessarily a 'true' yield stress [6–8]. The concept of the Bingham yield stress, however, can be considered as a useful engineering tool: it can be seen as the point at which solid-like behaviour is first seen when decreasing the applied stress on a Bingham fluid.

For a considerable number of powder type SCC mixes, using in Belgium readily available materials, the Bingham model results in negative values for the Bingham yield stress, which of course has no physical meaning. The effect is more pronounced when higher superplasticizer contents are added to the SCC mix, resulting in lower yield stresses [9,10]. In order to avoid the appearance of a negative yield stress, a shear thickening model must be used to describe this material's flow behaviour. The Herschel-Bulkley approach is mostly used to approximate the shear thickening flow behaviour of concrete [10–13]. In the last model, the relation $\tau(\dot{\gamma})$, after exceeding the Herschel-Bulkley yield stress $\tau_{0,HB}$, is described by a power law function:

$$\begin{cases} \tau = G^* \cdot \gamma (\text{or } \dot{\gamma} = 0) & \tau < \tau_{0,HB} \\ \tau = \tau_{0,HB} + K \cdot \dot{\gamma}^n & \tau \geq \tau_{0,HB} \end{cases} \quad (2)$$

Below the Herschel-Bulkley yield stress, the fluid behaves Hookean, while it is found that the SCC mix behaves shear thickening ($n>1$) above the yield stress [10]. K is called the 'consistency coefficient' (Pa·s^n), where n denotes the 'flow index' (−).

It should be mentioned explicitly that both the Bingham and the Herschel-Bulkley model should only be used for the description of the flow behaviour within the shear rate region actually tested during the rheological measurement. From this, it is clear that an appropriate shear rate region should be tested, in accordance with the practical shear rate region of interest (see also Section 5.2.1).

2.2. The wide-gap concentric cylinder rheometer

The used ConTec Visco5 wide-gap concentric cylinder rheometer (Fig. 1) is one of the most recent updates of the BML viscometer [14],

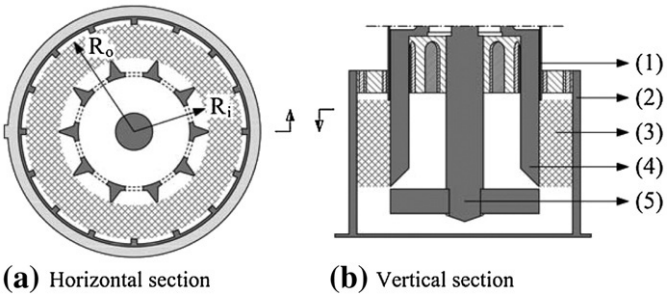

Fig. 1. Schematic cross-section of the ConTec Visco5 rheometer: (1) top ring; (2) outer cylinder, internal radius R_o = 145 mm; (3) sheared test material taken into consideration; (4) inner cylinder — free upper unit, external radius R_i = 100 mm; (5) inner cylinder — fixed bottom unit.

well designed for testing both (self-compacting) concrete and mortar (maximum aggregate size $D_{max} \leq 22$ mm). The outer cylinder rotates at an angular velocity $\Omega_o = 2\pi N$ (rad/s), while the inner cylinder is fixed to register the applied torque T (N·m) from the test material, i.e. the self-compacting concrete. In this way, this rheometer can be considered as a 'shear rate controlled' rheometer.

The measuring system consists of an outer cylinder (R_o = 145 mm), an inner cylinder unit (standard unit 'C-200': R_i = 100 mm) and a top ring. To avoid slippage between the cylinders and the test material, both the inner and outer cylinders are provided with protruding vanes [15–17]. With this, the dimensions R_i and R_o are relative to the extremities of the vanes (Fig. 1a). For a viscoplastic material, it is assumed that the material is held in the space between the vane blades so that it behaves like a rigid cylinder. Experimental observation confirms this assumption and is in accordance with experiences reported in literature [17–20]. Therefore, the eventual movement of particles between the vane blades is not investigated.

The top ring can be fitted over the inner cylinder, in order to ensure a constant height of the sheared test material. The inner cylinder is constructed as a two component unit (Fig. 1b): a bottom unit, which is fixed at the mounting point of the inner cylinder, and an upper unit, which is free to rotate against a load cell, registering the applied torque T from the test material. The arrangement of the two component inner cylinder will virtually eliminate the effect of 3D shearing at the bottom of the inner cylinder and therefore requires no special correction regarding possible bottom effects [21].

The following assumptions are made concerning the flow behaviour in the sheared test material, indicated by the shaded area in Fig. 1 (see [21,22] for more details):

- The flow between the two concentric cylinders is stable (i.e. laminar, without secondary flows) and symmetrical in z-direction.
- The flow behaviour is height independent (because bottom and top effects are eliminated by geometrical means: fixed bottom unit of inner cylinder and top ring).
- The flow is purely circular with angle independency (due to circular geometry of the concentric cylinder rheometer).
- The flow is steady state, i.e. time independent for the given measurement (because each measurement is applied in equilibrium conditions: equilibrium torque at each rotational velocity, see also Section 5.2).

2.3. 'Absolute rheometry': solutions for the 'Couette inverse problem'

Absolute rheometry involves the rheological measurement in 'absolute units of physics': it involves the determination of the flow behaviour in terms of shear rate $\dot{\gamma}$ (s^{-1}) and shear stress τ (Pa) instead of torque T (N·m) and rotational velocity N (rps). The most important benefit of absolute rheometry is that test results are independent of the particular rheometer and geometry used (concentric cylinders, plate-plate, cone-plate, …). It requires [23]:

- The test material to be subjected to a flow pattern that lends itself to a mathematical evaluation, whereby shear stresses and shear rates either at the walls or at representative points across the gap can be exactly calculated.
- The test conditions to be limited to the boundary conditions as mentioned above (assumptions concerning the flow behaviour).

In the case of a concentric cylinder rheometer, the derivation of the flow curve $\tau(\dot{\gamma})$ from the torque measurements $T(N)$ is often called the 'Couette inverse problem'. Three methods can be used to tackle this problem: (a) the integration method, where the type of constitutive equation is specified in advance and integrated to obtain the relation $T(N)$, which is fitted to the experimental data, (b) the Tikhonov regularization method, proposed by Yeow et al. [24] and (c) the wavelet-vaguelette decomposition method, proposed by Ancey [25].

Here, only the integration method is used for solving the Couette inverse problem. When using a wide-gap concentric cylinder, the solution is known as the '*Reiner-Riwlin' equation* for of a Bingham fluid [26], while the solution for a Herschel-Bulkley fluid has been reported only recently [1,22]. In this paper, only the resulting 'conversion' equations are given. For a detailed description of the derivation of those equations, the reader is referred to the relevant literature [1,21,26].

2.3.1. Integration approach of the Couette inverse problem for a Bingham and a Herschel-Bulkley fluid in a wide-gap concentric cylinder rheometer

The conversion equation for a Bingham fluid, i.e. the 'Reiner-Riwlin' equation, is given by:

$$T = \frac{4\pi h\tau_{0,B}}{\left(\frac{1}{R_i^2}-\frac{1}{R_o^2}\right)}\ln\left(\frac{R_o}{R_i}\right) + \frac{\mu 8\pi^2 h}{\left(\frac{1}{R_i^2}-\frac{1}{R_o^2}\right)}N \equiv G_B + H_B N \tag{3}$$

where G_B and H_B are respectively the flow resistance (N·m) and the viscosity factor (N·m·s) of a Bingham fluid, determined by a linear least square curve fitting (Section 5.2.2) of the experimental, steady state data $T(N)$ into $T=G_B+H_BN$.

The Bingham yield stress $\tau_{0,B}$ (Pa) and the plastic viscosity μ (Pa·s) are calculated as:

$$\tau_{0,B} = \frac{G_B}{4\pi h}\left(\frac{1}{R_i^2}-\frac{1}{R_o^2}\right)\frac{1}{\ln(R_o/R_i)} \tag{4}$$

$$\mu = \frac{H_B}{8\pi^2 h}\left(\frac{1}{R_i^2}-\frac{1}{R_o^2}\right) \tag{5}$$

For a Herschel-Bulkley fluid, the conversion equation is given by:

$$T = \frac{4\pi h\tau_{0,HB}}{\left(\frac{1}{R_i^2}-\frac{1}{R_o^2}\right)}\ln\left(\frac{R_o}{R_i}\right) + \frac{2^{2n+1}\pi^{n+1}hK}{n^n\left(\frac{1}{R_i^{2/n}}-\frac{1}{R_o^{2/n}}\right)^n}N^n \equiv G_{HB} + H_{HB}N^J \tag{6}$$

where G_{HB}, H_{HB} and J are respectively the flow resistance (N·m), the viscosity factor (N·m·s^J) and the flow index factor (−) of a Herschel-Bulkley fluid, determined by a nonlinear least square curve fitting (Section 5.2.2) of the experimental, steady state data $T(N)$ into $T=G_{HB}+H_{HB}N^J$.

The Herschel-Bulkley yield stress $\tau_{0,HB}$ (Pa), the consistency coefficient K (Pa·s^n) and the flow index n (−) are calculated as (see [1] for a detailed derivation of those expressions):

$$\tau_{0,HB} = \frac{G_{HB}}{4\pi h}\left(\frac{1}{R_i^2}-\frac{1}{R_o^2}\right)\frac{1}{\ln(R_o/R_i)} \tag{7}$$

$$K = \frac{H_{HB}}{2^{2n+1}\pi^{n+1}h}n^n\left(\frac{1}{R_i^{2/n}}-\frac{1}{R_o^{2/n}}\right)^n \tag{8}$$

$$n = J \tag{9}$$

It is clear from Eq. (7) that the Herschel-Bulkley yield stress can be calculated by using the same conversion equation as found for the Bingham yield stress (when replacing G_B by G_{HB}). Reason for this is the shear stress of a fluid being only dependent on the rheometer geometry and *not* on the nature of the fluid (at steady state) [21,22]. Note that Eq. (6) is valid for shear thickening ($n>1$), shear thinning ($n<1$) and even Bingham ($n=1$) fluids.

For a Hershel-Bulkley fluid, the rotational velocity N_P (rps) beneath which a plug is formed, is given by [1]:

$$N_P = \left(\frac{n}{4\pi}\right)\left(\frac{1}{R_i^{2/n}}-\frac{1}{R_o^{2/n}}\right)\sqrt[n]{\left(R_o^2 - \frac{2}{(1/R_i^2-1/R_o^2)}\ln\left(\frac{R_o}{R_i}\right)\right)\frac{\tau_{0,HB}}{K}} \tag{10a}$$

which can be simplified for a Bingham fluid into (see also [21]):

$$N_P = \left(\frac{1}{4\pi}\right)\left(\left(\frac{R_o^2}{R_i^2}-1\right)-2\ln\left(\frac{R_o}{R_i}\right)\right)\frac{\tau_{0,B}}{\mu} \tag{10b}$$

With a plug, a solid state arises ($\dot\gamma=0$) wherein the material rotates as a rigid body. When applying a stepwise decreasing rotational speed sequence (Section 5.2.1), the condition $\dot\gamma=0$, and so plug, will begin at the outer cylinder and propagate towards the inner cylinder as the angular velocity Ω_o ($=2\pi N$) is further decreased. In the transition zone between the viscoplastic and the solid state, slippage may possibly occur, resulting in smaller torque measurements than expected.

The above N_P-calculation is based on the assumption that the parameters $\tau_{0,HB}$, K and n are correct to begin with. However, it was found that the error, generated by plug flow, on the converted model parameters remained within their corresponding 95% confidence interval (Section 5.2.3) for all the rheological test results presented here (Section 6.2).

A disadvantage of both Eqs. (3) and (6) is that no information is given about the shear rate region actually tested by the $T(N)$ measurements. For this purpose, the following approximation formulae can be used for 'point by point' conversion of $T(N)$ into $\tau(\dot\gamma)$ [27]:

$$\tau = \frac{R_o^2+R_i^2}{R_o^2R_i^2}\frac{T}{4\pi h} \tag{11}$$

$$\dot\gamma = \frac{R_o^2+R_i^2}{R_o^2-R_i^2}2\pi N \tag{12}$$

Those equations are not dependent on any rheological model. However, they assume a linear velocity distribution across the gap between the two concentric cylinders, which is not fully true for a wide-gap concentric cylinder rheometer. When using this kind of rheometer, the assumption of a linear velocity distribution can only be used for preliminary design calculations [1].

2.3.2. Applicability of the conversion equations for absolute rheometry: determination of the rheological parameters of flower honey

As an illustration of the applicability of the above mentioned conversion equations for absolute rheometry, the rheological parameters of a light-coloured flower honey sample, provided by Meli plc (Belgium), were determined by two different types of rheometers:

- The ConTec Visco5 rheometer, with registration of the torque T (N·m) in function of the rotational velocity N (rps) (Section 2.2).
- The Physica MCR 501 rheometer (Anton Paar GmbH), with registration of the shear rate $\dot\gamma$ (s^{-1}) in function of the shear stress τ (Pa). Measurements were done with two different geometries: a parallel plate (PP25: plate diameter 25 mm, gap 1 mm) and a six-bladed vane (FL100/6W/Q1: R_i=11 mm, h=16 mm, cup CC27: R_o=12 mm). For each stress level, 20 $\tau(\dot\gamma)$ data points were recorded during a time interval of 200 s.

The temperature of the honey sample was set at 20 °C. The main specifications of the honey sample are:

- Specific gravity (at 20 °C): 1.50.
- Water content (at 20 °C): 15.0%.
- Monosaccharides (fructose + glucose): 70.0%.

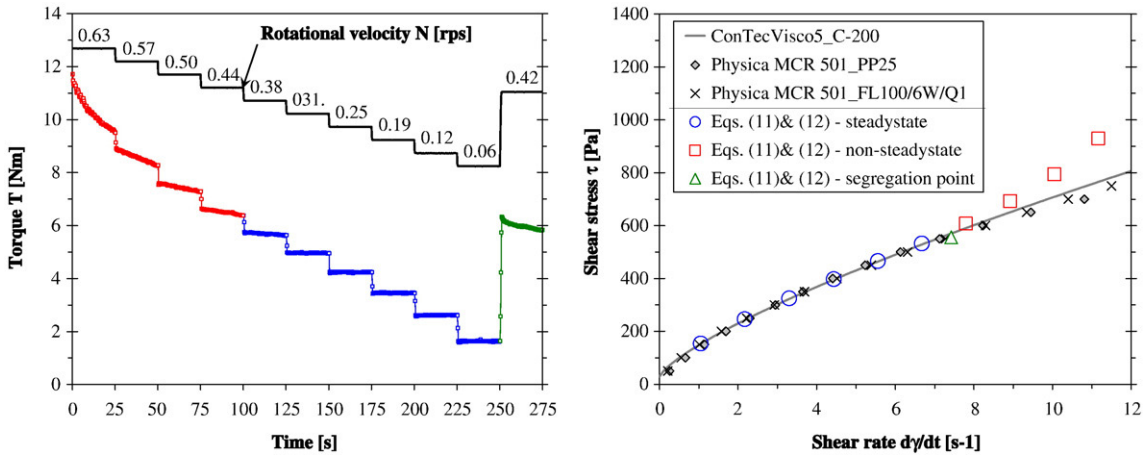

Fig. 2. Determination of rheological parameters of Meli flower honey at 20 °C with both the ConTec Visco5 (Eqs. (7)–(9)) and the Physica MCR 501 rheometer. The left figure shows the registered $T(N)$ data points with the ConTec Visco5 rheometer (N_P=0.003 rps).

- Disaccharides (sucrose): 1.0%.
- HMF (hydroxyl-methyl-furfural): 20 mg/kg

The rheological test results are presented in Fig. 2. Curve fitting of the steady state (T,N) data points measured with the ConTec Visco5 rheometer (Section 5.2), combined with the application of Eqs. (7)–(9), led to the following description of the flow behaviour of the Meli flower honey sample, for $1<\dot{\gamma}<11\ s^{-1}$ and applying the Herschel-Bulkley model:

$$\tau = \tau_{0,HB} + K\cdot\dot{\gamma}^{n} = 28.9 + 119.2\cdot\dot{\gamma}^{0.75} \quad (13)$$

It may be clear from Fig. 2 that the same flow curve was found for the three different geometries for $\dot{\gamma}<7.5\ s^{-1}$. For $\dot{\gamma}\geq 7.5\ s^{-1}$, the deviant behaviour observed in the ConTec Visco5 rheometer is explained by the non-steady state of the $T(N)$ measurements. Reason for this is the maximum sampling time interval provided by the rheometer's control software Freshwin at each rotational velocity (i.e. 25 s, as used in all experiments). This example illustrates the importance of not including non-steady state data points into the regression analysis (see also Section 5.2). Note that the measurements with the Physica MCR 501 indicate that Eq. (13) can still be used to describe the flow behaviour of the flower honey sample reasonably well for $7.5\leq\dot{\gamma}<11\ s^{-1}$.

3. Material characterisation

3.1. Aggregates

River aggregates (river gravel 4/14 and river sand 0/5), supplied by Gralex (Belgium), are used because of their most favourable, rounded shape for SCC production. They were oven dried before use. The use of a maximum aggregate size D_{max}=14 mm is in accordance with the required minimum gap size (=3·D_{max}) for concrete rheometry [5], in order to avoid interlocking of the aggregates, which will prevent flow. The specific gravities of the aggregates, determined according to EN 1097-6:2000, are listed in Table 1 while the grading curves, determined according to EN 933-1:1997 and EN 12620:2002, are presented in Fig. 3.

Table 1
Specific gravity SG (−) and Blaine fineness (m^2/kg) of constituent materials

Constituent material	SG	Blaine
River gravel 4/14	2.64	–
River sand 0/5	2.64	–
CEM I 52.5 R HES	3.13	600
CEM III/A 42.5 N LA	3.03	471
Limestone addition 1	2.70	338
Limestone addition 2	2.71	558
Quartzite addition	2.64	388
Fly ash	2.35	346
Water	1.00	–
Superplasticizer PCE 1	1.10	–
Superplasticizer PCE 2	1.08	–

3.2. Cement

Portland cement '*CEM I 52.5 R HES*' and blast furnace slag cement '*CEM III/A 42.5 N LA*', both according to EN 197-1:2000, are used. They are supplied by HeidelbergCement Group (CBR) (Belgium). The specific gravity and the Blaine fineness of both cement types are determined according to EN 1097-7:1999 and EN 196-6:1991, respectively. The results are listed in Table 1. The grading curves of both cement types are determined by means of laser diffraction, using the Sympatec Helos/Quixel apparatus (measuring range 1.8–350 µm). The results are presented in Fig. 4.

3.3. Mineral additions

Besides cement, different mineral additions were used as 'powder': (a) finely ground limestone addition 1: '*Calcitec 2001 S*' from Carmeuse (Belgium), (b) finely ground limestone addition 2: '*Betocarb P2 Mq*' from Omya Industries Inc. (France), (c) finely ground quartzite addition: '*Silfill*

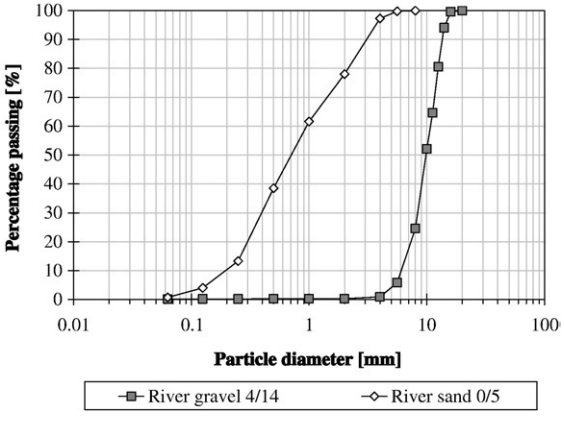

Fig. 3. Grading curves of aggregates.

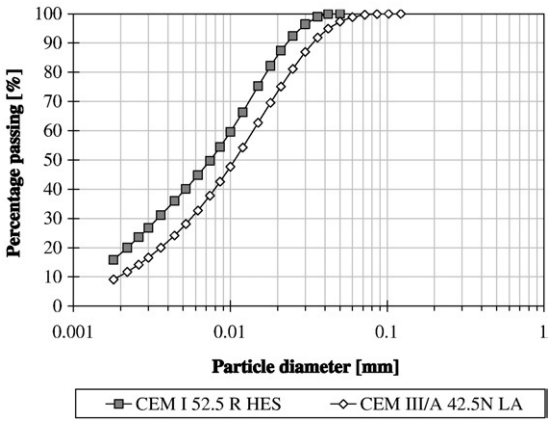

Fig. 4. Grading curves of both cement types.

3600 M' from Sibelco (Belgium), and (d) fly ash from Electrabel power station '*Langerlo*' (Belgium).

The mineral additions are characterised in the same way as both cement types: the specific gravity and the Blaine fineness of the mineral additions are listed in Table 1 and the grading curves are presented in Fig. 5.

3.4. Chemical admixtures

Two 'third generation' PCE superplasticizers are used: (a) PCE 1: '*Glenium 51 con 35%*' from BASF and (b) PCE 2: '*ViscoCrete-20 GOLD*' from Sika. The specific gravities of both superplasticizers (Table 1) are taken from their technical data sheets.

4. Mix proportions

In the experimental part of a Belgian research project concerning the influence of mineral additions and chemical admixtures in SCC on microcracking and durability [28], eight powder type SCC mixes and one TC mix are tested. For the SCC mixes, a constant amount of powder (cement and mineral addition) is considered: 600 kg/m^3. The compositions of the different concretes tested are given in Table 2. In the first part of this table (rheological behaviour), the mix compositions used for the study presented in this paper are given. Since the amount of PCE was different for each measurement, only the type of PCE used is indicated in this part by a cross marker (×). In the second part of the table (microcracking and durability), the final mix compositions chosen for the remaining experimental programme of the research project are given in order to illustrate fresh and hardened concrete properties of the different mixes (i.e. for a certain superplasticizer content, expressed in m-%, relative to the mass of cement).

Besides comparing TC to SCC, the influence of the following parameters is studied: type of mineral addition (two limestone additions with different fineness, one quartzite addition and one fly ash), type of chemical admixture (two 'third generation' PCE superplasticizers), type of cement (portland cement CEM I 52.5 R HES and blast furnace slag cement CEM III/A 42.5 N LA), cement/powder ratio (C/P=0.6 and C/P=0.5) and water/powder ratio (W/P=0.28 and W/P=0.33).

5. Experimental programme

5.1. Mixing procedure and test sequence

All mixes were prepared in a 50-l laboratory paddle-pan mixer (Eirich, type SKG1). First, all the dry material was put in the mixer. Then mixing was started. Tap water, set at 20 °C, was added during the first 15 s. One minute later, the mixer was paused for 15 s and the PCE superplasticizer was added. After PCE addition, mixing continued for 2 min.

After mixing, the slump-flow was measured and the rheological properties were determined with the ConTec Visco5 rheometer, placed in a climate room (20±2 °C and 54±5% R.H.). After testing, the concrete was poured back into the mixer, an extra amount of PCE was added and the concrete was mixed for another 2 min. This test sequence is repeated for each further measurement. The time between two consecutive measurements was about 40 min.

For each measurement, the amount of PCE superplasticizer added (PCE, in m-%, relative to the mass of cement), the particle volume fraction (Φ), the time after the addition of water (TW, in min) and the slump-flow (SF, in mm) are mentioned (Table 3, Section 6.2). The particle volume fraction Φ (−) is defined as:

$$\Phi = \frac{V_P}{V_P + V_m} \tag{14}$$

with V_P the volume of suspended particles and V_m the matrix volume.

Dealing with fresh concrete, the distinction between matrix and suspended particles is in fact a matter of choice, in contrast to the more traditional suspensions of spheres submerged in a Newtonian liquid. Here, the matrix of the fresh concrete mix is defined as the 0–2 mm mortar inside it, in accordance with literature concerned [21,29].

5.2. Rheological data processing

5.2.1. Data acquisition

To obtain the flow curve $T(N)$ with a maximum of steady state data points, the rotational velocity N is decreased in 10 steps (0.63→0.06 rps) of each 25 s (100 registration points), after a pre-shearing period of 10 s at 0.60 rps (in accordance with Wallevik [21], in order to finish thixotropic breakdown, and so to create uniform start conditions for all experiments, see also [30–35] for more information on this topic). For each velocity step, the average of torque T and rotational velocity N measured during the last 15 s can be seen as one (T,N) data point. If the torque for a certain point did not reach steady state, the point was omitted in further regression analysis.

Using Eq. (12) with $0.06<N<0.63$ rps, a shear rate region $1<\dot{\gamma}<11\ s^{-1}$ is found for the rheometer geometry used. The experiments revealed a higher probability of occurrence of experimental errors outside this shear rate region [1]:

- Lower shear rates can introduce the appearance of plug and thus of possible slippage in the transition zone from viscoplastic to solid state (resulting in smaller torque measurements than expected).

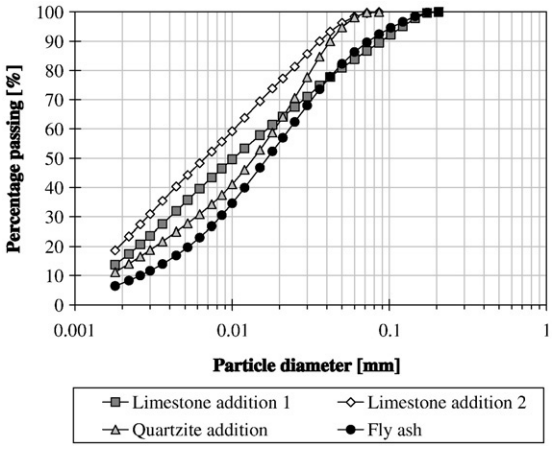

Fig. 5. Grading curves of mineral additions.

Table 2
Mix design (kg/m^3)

	TC20	SCC20	SCC21	SCC22	SCC23	SCC24	SCC25	SCC26	SCC27
Part 1: Rheological behaviour									
Gravel 4/14	1225	698	698	698	698	698	698	698	698
Sand 0/5	640	853	853	853	853	853	853	853	853
CEM I 52.5 R HES	360	360	360	360	360	360	–	300	360
CEM III/A 42.5 N LA	–	–	–	–	–	–	360	–	–
Limestone addition 1	–	240	–	–	–	240	240	300	240
Limestone addition 2	–	–	240	–	–	–	–	–	–
Quartzite addition	–	–	–	240	–	–	–	–	–
Fly ash	–	–	–	–	240	–	–	–	–
Water (at 20 °C)	165	165	165	165	165	165	165	165	198
Superplasticizer PCE 1	–	×	×	×	×	–	×	×	×
Superplasticizer PCE 2	–	–	–	–	–	×	–	–	–
W/C (−)	0.46	0.46	0.46	0.46	0.46	0.46	0.46	0.55	0.55
C/P (−)	1	0.6	0.6	0.6	0.6	0.6	0.6	0.5	0.6
W/P (−)	0.46	0.28	0.28	0.28	0.28	0.28	0.28	0.28	0.33
Part 2: Microcracking and durability									
PCE 1 (m-%)	–	1.25	1.39	1.39	1.88	–	0.97	1.25	0.69
PCE 2 (m-%)	–	–	–	–	–	1.39	–	–	–
Fresh concrete properties:									
Slump (mm)	*(5)*	–	–	–	–	–	–	–	–
Flow (mm)	320	–	–	–	–	–	–	–	–
Slump-flow (mm)	–	790	720	830	740	860	790	760	710
Slump-flow T50 (s)	–	3.8	4.4	3.7	5.8	2.4	3.9	3.3	1.3
V-funnel (s)	–	18.6	20.6	26.3	27.4	14.7	19.3	16.6	6.4
L-box // 3 rebars (−)	–	0.94	1.00	1.11	0.91	1.12	1.04	0.98	0.80
Sieve stability (%)	–	15	14	23	6	18	11	8	6
Air content (%)	1.7	1.9	1.6	1.4	2.6	1.0	1.8	1.6	1.7
Density (kg/m^3)	2361	2386	2375	2368	2322	2371	2328	2364	2343
Hardened concrete properties:									
$f_{c,cub150,28d}$ (N/mm^2)	58.6	87.9	77.7	82.5	76.5	77.0	65.3	69.6	65.7
Density (kg/m^3)	2382	2367	2340	2353	2303	2332	2335	2335	2312

Note: for Part 2, a new delivery batch of CEM I 52.5 R HES was used (specific gravity: 3.28, Blaine: 540 m^2/kg).

Moreover, structural reconstruction (coagulation and hydration of the cement particles) becomes more and more an influencing parameter at lower shear rates, due to the shear dependency of kinetics of dispersion and coagulation of the cement particles, possibly resulting in different rheological response and parameters obtained.

- Higher shear rates can introduce experimental errors due to e.g. particle migration (see [21] for further information on this topic).

However, the shear rate region actually tested is believed to approach the range of in situ shear behaviour of SCC casting: $\dot{\gamma}=10\ s^{-1}$ when leaving the concrete truck and $\dot{\gamma}=1\ s^{-1}$ near the end of concrete flow in the mould. Note that those values are only rough estimators of actual in situ shear behaviour (assuming a 10 cm thick concrete layer flowing at a speed of 1 m/s and 0.1 m/s respectively) since to date no exact method is established in order to measure 'true' in situ shear rates of concrete flow.

As an illustration of the data processing for the SCC mixes presented here, all registered rotational velocity and torque data points for mix SCC202 are shown in Fig. 6 (first point, at $N=0.63$ rps, omitted in further analysis due to non-steady state flow). When comparing Fig. 6 with Fig. 2, a greater fluctuation in recorded torque can be noticed. This is due to the larger aggregate particles present in the SCC mix, causing a larger and a more frequent momentum exchange between the aggregates. Additionally, bridges of those aggregates between the outer and inner cylinder are frequently formed, resulting in a direct torque transportation from the outer to the inner cylinder [21].

5.2.2. Regression analysis

Curve fitting, according to $T=G_{HB}+H_{HB}N^J$, of the steady state $T(N)$ data points is done by means of (non)linear regression analysis, using the Statistics Toolbox of Matlab® R2006a, based on the Levenberg-Marquardt algorithm. For each steady state, the last 60 registration points of both T and N are used for the regression analysis. In the case of Bingham (linear) behaviour, as it is for SCC242 and SCC261 (see below), the flow index factor equals unity: $J\equiv 1$ and curve fitting is done according to $T=G_B+H_BN$. The results for the model parameters G_B and H_B or G_{HB}, H_{HB} and J, as well as their 95% confidence interval half-widths (ΔG_B, ΔH_B, ΔG_{HB}, ΔH_{HB}, ΔJ), are presented in Table 3 (Section 6.2).

5.2.3. Confidence intervals of converted parameters: first order analysis

Eqs. (4) and (5) (Bingham case) or Eqs. (7)–(9) (Herschel-Bulkley case) are used to calculate the converted parameters $\tau_{0,B}$ and μ or $\tau_{0,HB}$, K and n, respectively. The 95% confidence interval half-widths for $\tau_{0,B}$, μ, $\tau_{0,HB}$ and n can be calculated directly, since the converted parameter is expressed as a linear function of the corresponding regression analysis parameter, resulting in the following 95% confidence interval half-width calculations (assuming that both the regression analysis parameter and the converted parameter are t-distributed):

$$\Delta\tau_{0,B} = \frac{\tau_{0,B}}{G_B}\Delta G_B \tag{15}$$

$$\Delta\mu = \frac{\mu}{H_B}\Delta H_B \tag{16}$$

$$\Delta\tau_{0,HB} = \frac{\tau_{0,HB}}{G_{HB}}\Delta G_{HB} \tag{17}$$

$$\Delta n = \Delta J \tag{18}$$

with ΔZ representing the 95% confidence interval half-width for the parameter Z.

Table 3
Model parameters of the flow curves for the SCC mixes

Mix	Mix characterisation				Model parameters $T(N)$ with 95% CI half-widths						Model parameters $\tau(\dot{\gamma})$ with 95% CI half-widths					
	PCE (m-%)	Φ (−)	TW (min)	SF (mm)	G_{HB} (N·m)	H_{HB} (N·m·s^J)	J (−)	ΔG_{HB} (N·m)	ΔH_{HB} (N·m·s^J)	ΔJ (−)	$\tau_{0,HB}$ (Pa)	K (Pa·s^n)	n (−)	$\Delta\tau_{0,HB}$ (Pa)	ΔK (Pa·s^n)	Δn (−)
TC20	0.00	0.523	/	/	/	/	/	/	/	/	/	/	/	/	/	/
SCC202	0.97	0.349	32	700	1.91	23.09	1.28	0.09	0.30	0.03	171.16	54.75	1.28	8.43	3.71	0.03
SCC204	1.25	0.348	80	740	0.68	13.12	1.39	0.05	0.15	0.03	60.92	23.29	1.39	4.53	1.59	0.03
SCC206	1.39	0.348	127	800	0.41	10.59	1.29	0.04	0.10	0.02	36.88	24.94	1.29	3.63	1.46	0.02
SCC207	1.67	0.348	164	850	0.32	9.13	1.57	0.03	0.11	0.03	28.38	9.67	1.57	2.51	0.68	0.03
SCC211	0.97	0.349	22	500	2.90	34.79	1.25	0.13	0.28	0.02	260.94	89.66	1.25	11.48	4.83	0.02
SCC212	1.25	0.349	70	710	0.91	15.92	1.60	0.05	0.22	0.03	81.36	15.47	1.60	4.59	1.18	0.03
SCC214	1.53	0.348	115	780	0.41	13.25	1.73	0.04	0.19	0.03	37.23	8.77	1.73	3.24	0.68	0.03
SCC217	1.94	0.348	200	860	0.37	10.87	1.81	0.03	0.19	0.04	32.95	5.72	1.81	2.88	0.53	0.04
SCC221	1.25	0.348	36	600	2.19	24.88	1.04	0.16	0.21	0.03	196.96	116.81	1.04	14.61	7.98	0.03
SCC222	1.53	0.347	84	700	0.74	22.51	1.42	0.06	0.27	0.02	66.42	36.37	1.42	5.66	2.09	0.02
SCC223	1.67	0.347	120	740	0.53	21.49	1.47	0.05	0.25	0.02	47.54	30.17	1.47	4.71	1.63	0.02
SCC225	1.94	0.347	194	810	0.38	20.78	1.54	0.05	0.26	0.02	34.49	23.68	1.54	4.27	1.34	0.02
SCC232	1.81	0.343	54	720	0.87	26.31	1.32	0.08	0.28	0.02	78.22	55.55	1.32	7.09	2.96	0.02
SCC233	2.08	0.343	92	750	0.55	24.08	1.35	0.08	0.28	0.02	49.82	47.79	1.35	6.84	2.78	0.02
SCC235	2.64	0.342	182	800	0.34	17.66	1.39	0.05	0.21	0.02	30.13	31.01	1.39	4.75	1.82	0.02
SCC242	1.25	0.348	54	510	2.19	14.75	1	0.04	0.11	–	196.44	78.37	1	3.47	0.58	–
SCC244	1.67	0.348	120	690	1.07	12.38	1.30	0.06	0.14	0.03	95.72	28.24	1.30	5.28	2.09	0.03
SCC246	2.08	0.347	182	830	0.43	10.70	1.65	0.04	0.17	0.03	38.96	8.89	1.65	3.21	0.76	0.03
SCC247	2.36	0.347	223	850	0.32	9.72	1.63	0.03	0.13	0.03	28.42	8.65	1.63	2.63	0.65	0.03
SCC252	1.25	0.347	60	610	1.20	25.77	1.12	0.12	0.20	0.02	107.69	98.07	1.12	10.96	5.49	0.02
SCC255	1.53	0.347	134	730	0.46	21.54	1.22	0.08	0.17	0.02	41.78	60.75	1.22	7.22	3.16	0.02
SCC256	1.81	0.346	177	810	0.37	18.34	1.43	0.05	0.21	0.02	33.28	28.35	1.43	4.37	1.58	0.02
SCC258	2.08	0.346	237	850	0.36	17.26	1.50	0.04	0.21	0.02	32.49	22.01	1.50	3.78	1.25	0.02
SCC261	1.17	0.348	24	560	2.94	16.28	1	0.05	0.13	–	264.08	86.52	1	4.67	0.71	–
SCC262	1.50	0.347	55	710	0.52	14.38	1.35	0.05	0.18	0.03	46.82	28.43	1.35	4.49	1.82	0.03
SCC264	2.00	0.347	125	830	0.29	13.22	1.49	0.03	0.16	0.02	25.93	17.36	1.49	2.86	0.96	0.02
SCC265	2.17	0.347	156	850	0.26	12.10	1.49	0.03	0.15	0.02	23.78	16.15	1.49	2.69	0.91	0.02
SCC271	0.56	0.338	15	490	2.22	8.61	1.12	0.06	0.13	0.04	199.65	32.04	1.12	5.37	2.85	0.04
SCC272	0.69	0.337	46	620	0.77	5.53	1.22	0.03	0.06	0.03	68.90	15.84	1.22	2.53	1.12	0.03
SCC273	0.83	0.337	73	750	0.45	4.12	1.45	0.02	0.07	0.04	40.38	6.01	1.45	1.79	0.57	0.04
SCC274	0.97	0.337	103	850	0.30	3.61	1.67	0.02	0.08	0.05	27.27	2.84	1.67	1.43	0.33	0.05

PCE = PCE superplasticizer content; Φ = particle volume fraction of aggregates, Eq. (14); TW = time after water addition; SF = slump-flow; CI = confidence interval.

On the other hand, it is clear from Eq. (8) that the converted parameter K is a nonlinear function of the two parameters H_{HB} and n. The 95% confidence interval half-width for K is calculated by means of a first order analysis, i.e. the nonlinear function $K=f(H_{HB},n)$ is approximated by a linear function (its first order Taylor series expansion) in the neighbourhood of the expected values for H_{HB} and n in order to calculate the variance of K. In this way, the approximate variance of K is given by:

$$\sigma_K^2 \approx \left(\frac{\partial K}{\partial H_{HB}}\right)^2 \sigma_{H_{HB}}^2 + 2\left(\frac{\partial K}{\partial H_{HB}}\right)\left(\frac{\partial K}{\partial n}\right)\sigma_{H_{HB}n} + \left(\frac{\partial K}{\partial n}\right)^2 \sigma_n^2 \quad (19)$$

with $\sigma^2_{H_{HB}}$ the variance of H_{HB}, σ_n^2 the variance of n and $\sigma_{H_{HB}n}$ the covariance of H_{HB} and n, all given by the nonlinear regression analysis (by using Eq. (9): $n=J$).

Since the converted parameter K is assumed to be t-distributed, with $(n-3)$ degrees of freedom (in this context, n stands for the total number of steady state $T(N)$ data points, e.g. $n=9\times60=540$ for SCC202, see also Fig. 6), the 95% confidence interval half-width for K is calculated as:

$$\Delta K = t_{0.975,n-3}\sigma_K \approx t_{0.975,n-3}\sqrt{\left(\frac{\partial K}{\partial H_{HB}}\right)^2 \sigma_{H_{HB}}^2 + 2\left(\frac{\partial K}{\partial H_{HB}}\right)\left(\frac{\partial K}{\partial n}\right)\sigma_{H_{HB}n} + \left(\frac{\partial K}{\partial n}\right)^2 \sigma_n^2} \quad (20)$$

with $t_{0.975,n-3}$ the 0.975 quantile of the Student's t-distribution with $(n-3)$ degrees of freedom and, after applying some simple algebra, $\partial K/\partial H_{HB}$ and $\partial K/\partial n$ given by:

$$\frac{\partial K}{\partial H_{HB}} = \frac{K}{H_{HB}} \quad (21)$$

$$\frac{\partial K}{\partial n} = K\left\{1 + \ln\left(\frac{n}{4\pi}\left(\frac{1}{R_i^{2/n}} - \frac{1}{R_o^{2/n}}\right)\right) + \frac{2}{n}\left(\frac{R_o^{2/n}\ln(R_i) - R_i^{2/n}\ln(R_o)}{R_o^{2/n} - R_i^{2/n}}\right)\right\} \quad (22)$$

6. Rheological measurements: results and discussion

6.1. Traditionally vibrated concrete mix TC20

The traditionally vibrated concrete mix TC20 was too stiff to be tested in the ConTec Visco5 rheometer (slump <10 mm, flow=320 mm, according to EN 12350-2:1999 and EN 12350-5:1999, respectively). Moreover, the slump of 10 mm << 100 mm indicates that TC20 cannot be considered as a fluid [5]. For this stiff mix, the effect of 'particle migration' during the test was clearly noticeable, as shown in Fig. 7. Three physical phenomena are accountable for the particle migration in this case [21]:

- ***Collision effect.*** In the case of 'freely moving' particles (i.e. if $D_{flow}/D_{max} \geq 8$, with D_{flow} the characteristic flow thickness, $D_{flow}=\Delta R=R_o-R_i$, and D_{max} the maximum aggregate size), the suspended particles (>2 mm) are 'pushed' away by collisions from the region of highest collision rate (i.e. at the surface of the inner cylinder) towards the outer cylinder and into the serrated region of the inner cylinder, leaving

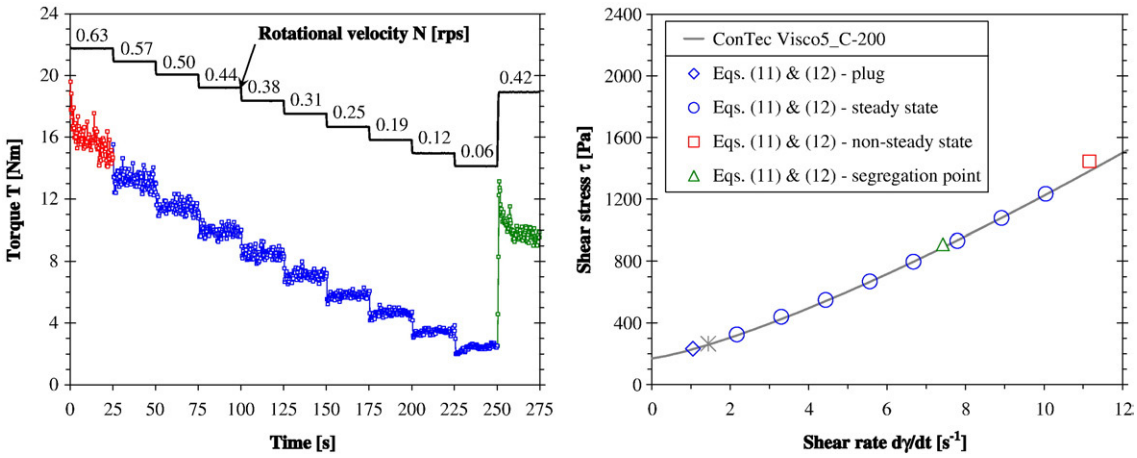

Fig. 6. Determination of rheological parameters of SCC202 at 20 °C with the ConTec Visco5 rheometer, calculated from Eqs. (7)–(9). The left figure shows the registered $T(N)$ data points (∗:indication of the shear rate when a plug starts to form (N_P=0.08 rps)).

behind a concrete that is very rich in mortar in the region near the inner cylinder.

- ***Confinement effect.*** At lower D_{flow}/D_{max} ratios (as it is the case for the ConTec Visco5 rheometer equipped with the C-200 standard unit: D_{flow}/D_{max}=45/14≈3), harder and more frequent collisions between the suspended particles occur, resulting in a stronger 'pushing' mechanism than anticipated by the previous effect.
- ***Dilatancy effect.*** In case of densely packed suspended particles (as it is the case for TC20: Φ=0.523), the suspended particle distribution Φ must change in order to permit the suspended particles to flow next to each other, resulting in a 'suction' of matrix into the region near the inner cylinder surface. Consequently, the suspended particles must be pushed in the opposite direction due to the law of conservation of matter (i.e. towards the outer cylinder and into the serrated region of the inner cylinder).

The effect of particle migration is far less present for the SCC mixes presented in this paper, due to:

- An increased average distance between the suspended particles. Reasons for this are the lower particle volume fraction (Φ=0.337 à 0.349 for the SCC mixes while Φ=0.523 for TC20) and the increased amount of powder (P=600 kg/m^3 for the SCC mixes while P=360 kg/m^3 for TC20).
- A better lubrication between the suspended particles because of the superplasticizer addition in case of the SCC mixes.

6.2. Powder type SCC mixes

The resulting flow curves $\tau(\dot{\gamma})$ for the SCC mixes are shown in Fig. 8. In this figure, the point markers indicate the results for the approximate 'point by point' conversions according to Eqs. (11) and (12) (◊: plug flow, ∗: indication of the shear rate when a plug starts to form (N_P), ○: steady state, and □: non-steady state). The corresponding model parameters $\tau_{0,B}$ and μ or $\tau_{0,HB}$, K and n, as well as their 95% confidence interval half-widths ($\Delta\tau_{0,B}$, $\Delta\mu$, $\Delta\tau_{0,HB}$, ΔK, Δn), are presented in Table 3. Hereafter, SCC20 (limestone addition 1, PCE 1, portland cement CEM I 52.5 R HES, C/P=0.6 and W/P=0.28) is used as reference mix when comparing the influencing parameters, as given in Section 4.

6.2.1. Influence of chemical admixtures

In general, increasing the PCE content resulted in a decrease of both the yield stress $\tau_{0,HB}$ and the consistency factor K and in an increase of the flow index n for all powder type SCC mixes presented in this paper. The decreased yield stress can be attributed to the dispersing action of the PCE superplasticizer, resulting in a more

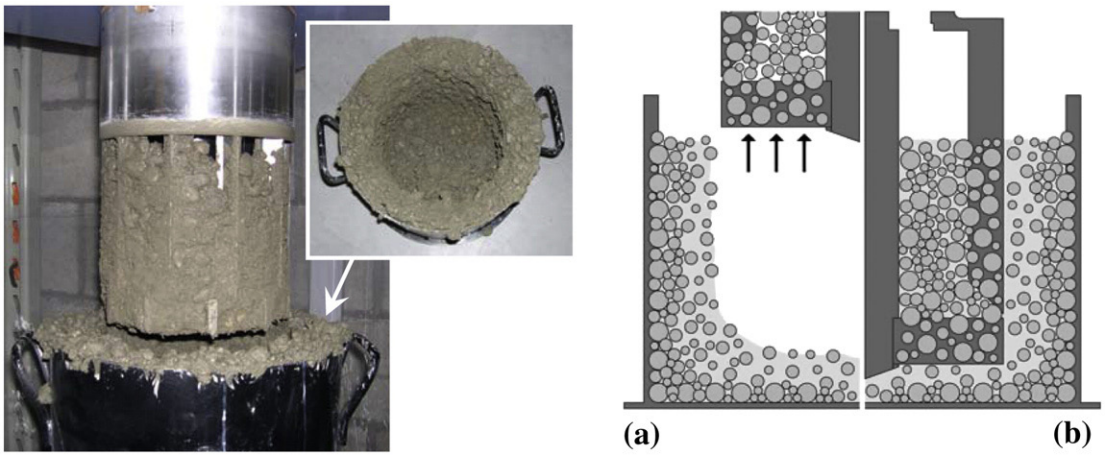

Fig. 7. Particle migration inside the ConTec Visco5 rheometer for the stiff mix TC20. Overview after measurement (left) and schematic illustration of particle distribution $\Phi = \Phi(r,z)$, after (a) and during (b) measurement (right, after [20]).

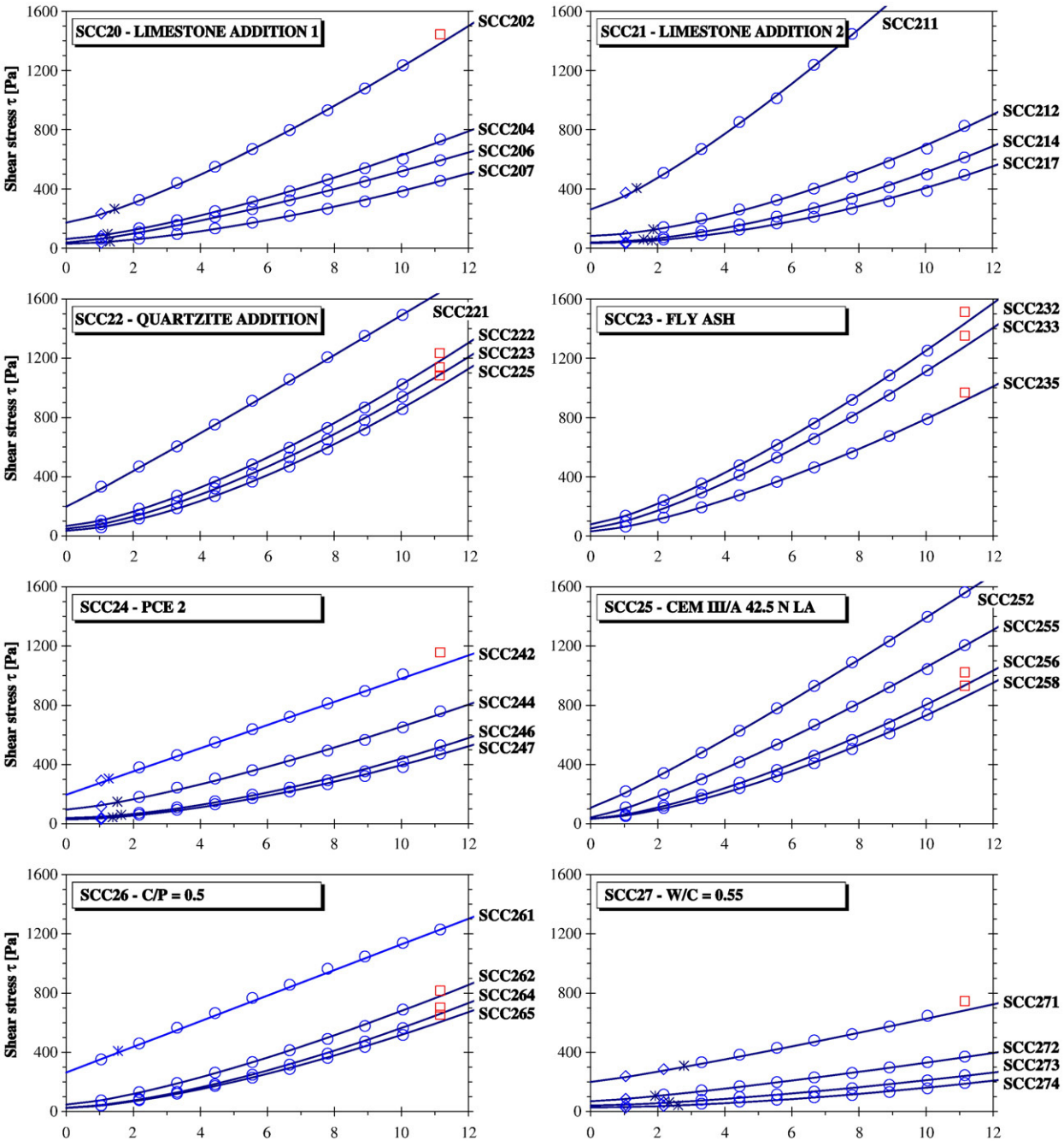

Fig. 8. Flow curves $\tau(\dot{\gamma})$ for the SCC mixes, calculated from Eqs. (7)–(9). The point markers indicate the results for the approximate conversions according to Eqs. (11) and (12) (◊: plug flow, ∗: indication of the shear rate when a plug starts to form (N_P), ○: steady state, and □: non-steady state).

deflocculated state. Besides, results indicated that the phenomena accountable for the shear thickening effect of superplasticizers on the rheological behaviour of cement pastes [13] can also be used in order to explain the influence of the PCE superplasticizer addition on the shear thickening behaviour of powder type SCC. Or else, the effect of PCE addition on the shear thickening behaviour of powder type SCC seems to be mainly influenced by the rheological behaviour of its cement paste. The following phenomena can be related to the shear thickening effect due to the presence of superplasticizer [13]:

- The increase of shear rate possibly enhances the disorder, not only between the powder particles, but also within the polymeric chains of the superplasticizer. According to the order-disorder transition theory of Hoffman [36], a more disordered state results in a higher degree of particles jamming, involving cluster formation both with and without direct particle contact, and hence resulting in an increased (coefficient of) viscosity η ($=\tau/\dot{\gamma}$).
- The increase of shear rate possibly tears off some part of the adsorbed superplasticizer, resulting in: (a) an increased disorder state of the free water, increasing its viscosity and possibly making it shear thickening and (b) an increased probability of interparticular bonds between the powder particles (cluster theory of Brady and Bossis [37]), jamming the flow and hence increasing the viscosity η.

It should be mentioned explicitly that those phenomena were presented as hypothetical in [13], and thus so they are here. More

work in this field is needed in order to explain the interaction between the (micro)structure and the rheological behaviour.

When replacing PCE 1 by PCE 2 (SCC24), the time after water addition TW (Table 3) should be kept in mind when comparing the results. In this way, a strong increase of both the yield stress $\tau_{0,HB}$ and the consistency factor K and a decrease of the flow index n is observed for PCE 2, although both superplasticizers were supposed to be of equal 'efficiency' (as indicated by their dry mass content: 36.5% for PCE 1 and 38.8% for PCE 2). The different behaviour of both superplasticizers is most probably due to a different molecular design of both superplasticizers.

6.2.2. Influence of mineral additions

Concerning the influence of the mineral addition, both the PCE content and the time after water addition TW (Table 3) should be kept in mind when comparing the results. Besides, it should be mentioned explicitly that the amount of powder was fixed at a constant *mass* of 600 kg per cubic concrete, resulting in a different powder *volume* when a mineral addition with a different specific gravity (Table 1) was used. In this respect, it can be noted that a higher powder volume results in a higher viscosity η, as illustrated by e.g. the well-known Krieger-Dougerthy equation:

$$\frac{\eta}{\eta_m} = \left(1 - \frac{\Phi}{\Phi_m}\right)^{-[\eta]\Phi_m} \quad (23)$$

with η the viscosity of the suspension (Pa·s), η_m the viscosity of the matrix (Pa·s), Φ the suspended particle *volume* fraction, according to Eq. (14) (−), Φ_m the maximum suspended particle *volume* fraction (−) and $[\eta]$ the intrinsic viscosity of the matrix (−) (=2.5 for hard, monodispersed spheres) [5,7].

Eq. (23) can be used both for the concrete mix (with the aggregates >2 mm as the suspended particles) and for its matrix (i.e. the 0–2 mortar inside it). In the latter case, the aggregates ≤2 mm and all the powder material are considered as the suspended particles into a 'matrix' of water and superplasticizer. Since the amount of aggregates was kept constant for all the SCC mixes considered here, the differences in viscosity η of the relevant SCC mixes can be linked to the different volumes of the specific mineral addition used. The volumes of limestone addition 1 (LS 1, SCC20), limestone addition 2 (LS 2, SCC21), quartzite addition (Q, SCC22) and fly ash (FA, SCC23) are 8.89, 8.86, 9.09 and 10.21 vol.% (relative to the total concrete volume), respectively.

Moreover, a higher powder volume results in a lower content of free water (since the total amount of water was fixed for the relevant SCC mixes), resulting in an increased disorder state of this free water and thus increasing its viscosity.

Cyr et al [13] found that mineral additions, as replacements of different amounts of cement, can modify the intensity of shear thickening (as indicated by the flow index n) compared to plain cement pastes. In accordance with their results, we also observed that the inert Q does not alter the intensity of shear thickening. For the other mineral additions used, test results revealed an increased intensity for both LS 1 and LS 2, while a decreased intensity was found when FA was used. Besides, it was found that the finer LS 2 (Blaine fineness 558 m^2/kg) resulted in higher shear thickening intensity compared to LS 1 (Blaine fineness 338 m^2/kg). The latter phenomenon can be explained by the decreased free water content, increasing its disorder state and thus increasing its viscosity and possibly making it shear thickening.

6.2.3. Influence of cement type, cement/powder ratio (C/P) and water/powder ratio (W/P)

When portland cement CEM I 52.5 R HES is replaced by blast furnace slag cement CEM III/A 42.5 N LA (SCC25), a nearly double consistency coefficient K is found for comparable PCE content and time after water addition, while both the yield stress $\tau_{0,HB}$ and the flow index n were comparable. The same phenomenon was also observed, although less pronounced, when the C/P ratio decreased from 0.6 to 0.5 (SCC26). Also in those cases, the explanation can be found in the higher powder volume for mixes SCC25 (11.88 + 8.89 = 20.77 vol.%) and SCC26 (9.58 + 11.11 = 20.69 vol.%) compared to SCC20 (11.50 + 8.89 = 20.39 vol.%, all relative to the total concrete volume), resulting in a higher viscosity η. In case of the cement replacement, test results revealed that the effect of the lower cement fineness is overshadowed by the increased powder volume fraction.

Increasing the water content (SCC27, W/P = 0.33) resulted in a strong decrease of both the yield stress $\tau_{0,HB}$ and the consistency factor K, in accordance with literature data [38], compared to SCC20 (W/P = 0.28). Increasing the water content results in both a decreased viscosity of the liquid phase (decreased concentration of superplasticizer) and a decreased suspended particle volume fraction of the powder, resulting in a lower viscosity of the matrix and thus in a lower viscosity of the concrete mix (since the amount of aggregates was also held constant for this mix). Moreover, also a lower flow index n was found, most probably due to the increased order between the powder particles and within the polymeric chains of the superplasticizer.

7. Conclusions

The influence of mineral additions and chemical admixtures on the shear thickening behaviour of powder type SCC, using in Belgium readily available materials, was studied by using a wide-gap concentric cylinder rheometer. Special care was taken to eliminate possible experimental errors introducing a misinterpretation of the obtained torque measurements $T(N)$. Such experimental errors include non-steady state flow, plug flow and particle migration. Test results indicated that a shear thickening behaviour was often found for the SCC mixes studied here. In order to describe the flow curves independently of the type of rheometer used, the Couette inverse problem for a shear thickening material tested in a wide-gap concentric cylinder rheometer had to be solved. Calculations of the 95% confidence intervals of the converted parameters are presented in this paper.

The influence of the following parameters was studied in order to point out the occurrence of shear thickening behaviour in (powder type) SCC: type of mineral addition, type and dosage of PCE superplasticizer, type of cement, C/P ratio and W/P ratio. The following conclusions can be drawn:

1. The Herschel-Bulkley yield stress $\tau_{0,HB}$, the consistency coefficient K and the flow index n are found to be reliable, absolute rheometry parameters (in the shear rate region actually tested). The wide-gap concentric cylinder rheometer provides a reproducible test procedure, from which the parameters and their influencing factors can be derived.
2. According to our experimental results, the PCE superplasticizer has a strong influence on the shear thickening behaviour of powder type SCC. Besides, it was found that the molecular design of the PCE superplasticizer has a non-negligible impact on the shear thickening effect.
3. The intensity of the shear thickening effect can be modified by the nature and fineness of the mineral addition used. It was found that the limestone, quartzite and fly ash addition used in this research project, respectively, increase, unalter and decrease the shear thickening intensity. Increasing the fineness of the limestone addition resulted in a higher shear thickening intensity.
4. The replacement of portland cement CEM I 52.5 R HES by blast furnace slag cement CEM III/A 42.5 N LA does not influence the shear thickening behaviour.
5. Increasing the water content results in decreased shear thickening effect.
6. The powder volume and the available amount of free water have a major impact on the viscosity of the powder type SCC mixes.

Increasing the powder volume, or decreasing the amount of free water (e.g. when increasing the fineness of the limestone addition) results in an increased viscosity of the SCC mix.

Microstructural interpretations of the rheological behaviour are attempted with the help of the order-disorder transition theory and the cluster theory, complemented with local mechanical actions caused by the shear effect.

Nomenclature

Symbol	Description	Unit
Latin letters		
C/P	Cement/powder ratio by mass	(−)
D_{flow}	Characteristic thickness of the flow = $\Delta R = R_o - R_i$	(mm)
D_{max}	Maximum aggregate size	(mm)
G^*	(Complex) shear modulus	(Pa)
G_B	Flow resistance of Bingham fluids	(N·m)
G_{HB}	Flow resistance of Herschel-Bulkley fluids	(N·m)
H_B	Viscosity factor of Bingham fluids	(N·m·s)
H_{HB}	Viscosity factor of Herschel-Bulkley fluids	(N·m·s^J)
J	Flow index factor of Herschel-Bulkley fluids	(−)
K	Consistency coefficient of Herschel-Bulkley fluids	(Pa·s^n)
n	Flow index of Herschel-Bulkley fluids	(−)
N	Rotational velocity of the outer cylinder	(rps)
N_P	Rotational velocity of the outer cylinder beneath which a plug is formed in the test material	(rps)
PCE	Polycarboxylate ether (superplasticizer)	
R_i	External radius of the inner cylinder	(m or mm)
R_o	Internal radius of the outer cylinder	(m or mm)
SF	Slump-flow	(mm)
SG	Specific gravity	(−)
T	Torque, measured on inner cylinder	(N·m)
TW	Time after water addition	(min)
V_m	Matrix volume	(l)
V_p	Volume of suspended particles	(l)
W/C	Water/cement ratio by mass	(−)
W/P	Water/powder ratio by mass	(−)
Greek letters		
ΔZ	95% confidence interval half-width for parameter Z	
Φ	Particle volume fraction = $V_P/(V_P+V_m)$	(−)
γ	Shear strain	(−)
$\dot{\gamma}$	Shear rate = $d\gamma/dt$	(s^{-1})
η	(Coefficient of) viscosity of the suspension = $\tau/\dot{\gamma}$	(Pa·s)
η_m	(Coefficient of) viscosity of the matrix	(Pa·s)
$[\eta]$	Intrinsic viscosity (=2.5 for spheres)	(−)
μ	Plastic viscosity of Bingham fluids	(Pa·s)
ρ	Density	(kg/m^3)
τ	Shear stress	(Pa)
$\tau_{0,B}$	Bingham yield stress	(Pa)
$\tau_{0,HB}$	Herschel-Bulkley yield stress	(Pa)
Ω_o	Angular velocity of the outer cylinder = $2\pi N$	(rad/s)

Acknowledgments

The financial support of the Research Programme of the Research Foundation – Flanders (FWO) is greatly acknowledged. The Applied Rheology and Polymer Processing Section of the Department of Chemical Engineering (K.U.Leuven) is greatly acknowledged for their contributions to the rheological description of the honey sample with the Physica MCR 501 rheometer.

References

[1] G. Heirman, L. Vandewalle, D. Van Gemert, Ó. Wallevik, Integration approach of the Couette inverse problem of powder type self-compacting concrete in a wide-gap concentric cylinder rheometer, J. Non-Newton. Fluid Mech. 150 (2–3) (2008) 93–103.
[2] BIBM, CEMBUREAU, EFCA, EFNARC, ERMCO, The European Guidelines for Self-Compacting Concrete: Specification, Production and Use, 2005, 63 pp.
[3] G. De Schutter, P.J.M. Bartos, P. Domone, J. Gibbs (Eds.), Self-Compacting Concrete, Whittles Publishing, Dunbeath, Caithness (UK), 2008, 312 pp.
[4] G. De Schutter, Guidelines for Testing Fresh Self-Compacting Concrete (European research project GRD2-2000-30024: Measurements of Properties of Fresh Self-Compacting Concrete), 2005 23 pp.
[5] C.F. Ferraris, F. de Larrard, N. Martys, Fresh concrete rheology: recent developments, in: S. Mindess, J.P. Skalny (Eds.), Materials of Science VI. Wiley, American Ceramic Society, Westerville (US), 2001, pp. 215–241.
[6] H.A. Barnes, The yield stress — a review or 'παντα ρει' — everything flows? J. Non-Newton. Fluid Mech. 81 (1–2) (1999) 133–178.
[7] C.W. Macosko, Rheology — Principles, Measurements, and Applications, Wiley–VCH, New York (US), 1994.
[8] Ph. Coussot, Rheometry of Pastes, Suspensions, and Granular Materials: Applications in Industry and Environment, John Wiley & Sons, New Jersey (US), 2005 291 pp.
[9] D. Feys, G. De Schutter, R. Verhoeven, Fresh self compacting concrete, a shear thickening material, Cem. Concr. Res. 38 (7) (2008) 920–929.
[10] G. Heirman, L. Vandewalle, D. Van Gemert, D. Feys, G. De Schutter, B. Desmet, J. Vantomme, Influence of mineral additions and chemical admixtures on the rheological behaviour of powder type SCC, in: G. De Schutter, V. Boel (Eds.), SCC2007 — Proc. of the 5th Int. RILEM Symp. on Self-Compacting Concrete, Ghent, 3–5 September 2007. RILEM Publications SARL, Bagneux (FR), 2007, pp. 329–334.
[11] C.F. Ferraris, F. de Larrard, Testing and Modelling of Fresh Concrete Rheology (NISTIR 6094), 1998 61 pp.
[12] F. de Larrard, C.F. Ferraris, T. Sedran, Fresh concrete: a Herschel-Bulkley material, Mater. Struct. 31 (7) (1998) 494–498.
[13] M. Cyr, C. Legrand, M. Mouret, Study of the shear thickening effect of superplasticizers on the rheological behaviour of cement pastes containing or not mineral additives, Cem. Concr. Res. 30 (9) (2000) 1477–1483.
[14] Ó. Wallevik, The rheology of fresh concrete and its application on concrete with and without silica fume, PhD dissertation, NTNU Trondheim (NO), 1990, 185 pp. <only available in Norwegian>.
[15] N.Q. Dzuy, D.V. Boger, Yield stress measurements for concentrated suspensions, J. Rheol. 27 (4) (1983) 321–349.
[16] A.W. Saak, H.M. Jennings, S.P. Shah, The influence of wall slip on yield stress and viscoelastic measurements of cement paste, Cem. Concr. Res. 31 (2) (2001) 205–212.
[17] J.E. Wallevik, Thixotropic investigation on cement paste: experimental and numerical approach, J. Non-Newton. Fluid Mech. 132 (1–3) (2005) 86–99.
[18] M. Keentok, J.F. Milthorpe, E. O'Donovan, On the shearing zone around rotating vanes in plastic liquids: theory and experiment, J. Non-Newton. Fluid Mech. 17 (1) (1985) 23–25.
[19] J. Yan, A.E. James, The yield surface of viscoelastic and plastic fluids in a vane viscometer, J. Non-Newton. Fluid Mech. 70 (3) (1997) 237–253.
[20] H.A. Barnes, Q.D. Nguyen, Rotating vane rheometry — a review, J. Non-Newton. Fluid Mech. 98 (1) (2001) 1–14.
[21] J.E. Wallevik, Rheology of particle suspensions, fresh concrete, mortar and cement paste with various types of lignosulfonates, PhD dissertation, NTNU Trondheim (NO), 2003, 397 pp.
[22] G. Heirman, L. Vandewalle, D. Van Gemert, Ó. Wallevik, N. Cauberg, Contribution to the solution of the Couette inverse problem for Herschel-Bulkley fluids by means of the integration method, in: J. Marchand, B. Bissonnette, R. Gagné, M. Jolin, F. Paradis (Eds.), Proc. of the 2nd Int. RILEM Symp. on Advances in Concrete Through Science and Engineering, Quebec City, RILEM Publications SARL, Bagneux (FR), September 11–13 2006, 15 pp. <on CD-ROM>.
[23] G. Schramm, A Practical Approach to Rheology and Rheometry, Thermo Haake GmbH, Karlsruhe (DE), 2002.
[24] Y. Yeow, W. Ko, P. Tang, Solving the inverse problem of Couette viscometry by Tikhonov regularization, J. Rheol. 44 (6) (2000) 1335–1351.
[25] C. Ancey, Solving the Couette inverse problem using a wavelet-vaguelette decomposition, J. Rheol. 49 (2) (2005) 441–460.
[26] M. Reiner, Deformation and Flow — an Elementary Introduction to Theoretical Rheology, H.K. Lewis & Co. Ltd, London (GB), 1949.
[27] M. Nehdi, M.A. Rahman, Effect of geometry and surface friction of test accessory on oscillatory rheological properties of cement pastes, ACI Mater. J. 101 (5) (2004) 416–424.
[28] G. Heirman, L. Vandewalle, D. Van Gemert, J. Elsen, V. Boel, K. Audenaert, G. De Schutter, B. Desmet, J. Vantomme, Influence of mineral additions and chemical admixtures in SCC on microcracking and durability: overview of a Belgian research project, in: G. De Schutter, V. Boel (Eds.), SCC2007 — Proc. of the 5th Int. RILEM Symp. on Self-Compacting Concrete, Ghent, RILEM Publications SARL, Bagneux (FR), September 3–5 2007, pp. 773–778.
[29] H.A. Barnes, J.F. Hutton, An Introduction to Rheology, Elsevier, Oxford (GB), 1989 210 pp.
[30] M.R. Geiker, M. Brandl, L.N. Thrane, D.H. Bager, Ó. Wallevik, The effect of measuring procedure on the apparent rheological properties of self-compacting concrete, Cem. Concr. Res. 32 (11) (2002) 1791–1795.
[31] N. Roussel, Steady and transient flow behaviour of fresh cement pastes, Cem. Concr. Res. 35 (9) (2005) 1656–1664.
[32] S. Jarny, N. Roussel, S. Rodts, F. Bertrand, R. Le Roy, P. Coussot, Rheological behaviour of cement pastes from MRI velocimetry, Cem. Concr. Res. 35 (10) (2005) 1873–1881.
[33] N. Roussel, A thixotropy model for fresh fluid concretes: theory, validation and applications, Cem. Concr. Res. 36 (10) (2006) 1797–1806.
[34] H. Vikkan, H. Justnes, Rheology of cementitious paste with silica fume or limestone, Cem. Concr. Res. 37 (11) (2007) 1512–1517.
[35] J.E. Wallevik, Rheological properties of cement paste: Thixotropic behaviour and structural breakdown, Cem. Concr. Res. 39 (1) (2009) 14–29.
[36] R.L. Hoffman, Explanations for the cause of shear thickening in concentrated colloidal suspensions, J. Rheol. 42 (1) (1998) 111–123.
[37] J.F. Brady, G. Bossis, The rheology of concentrated suspensions of spheres in simple shear flow by numerical simulation, J. Fluid Mech. 155 (1985) 105–129.
[38] Ó. Wallevik, Course on rheology of coarse particle suspensions, such as cement paste, mortar and concrete, IBRI, Reykjavik (IS), Limelette (BE), October 7–8 2004.